

Bowling Green State University  
**ScholarWorks@BGSU**

---

Chemistry Faculty Publications

Chemistry

---

10-2008

## Fluorescence Sensor Array For Metal Ion Detection Based On Various Coordination Chemistries: General Performance And Potential Application


Zhuo Wang

Manuel A. Palacios

Pavel Anzenbacher Jr.

*Bowling Green State University*, [pavel@bgsu.edu](mailto:pavel@bgsu.edu)

Follow this and additional works at: [https://scholarworks.bgsu.edu/chem\\_pub](https://scholarworks.bgsu.edu/chem_pub)

 Part of the [Chemistry Commons](#)

---

### Repository Citation

Wang, Zhuo; Palacios, Manuel A.; and Anzenbacher, Pavel Jr., "Fluorescence Sensor Array For Metal Ion Detection Based On Various Coordination Chemistries: General Performance And Potential Application" (2008). *Chemistry Faculty Publications*. 150.  
[https://scholarworks.bgsu.edu/chem\\_pub/150](https://scholarworks.bgsu.edu/chem_pub/150)

This Article is brought to you for free and open access by the Chemistry at ScholarWorks@BGSU. It has been accepted for inclusion in Chemistry Faculty Publications by an authorized administrator of ScholarWorks@BGSU.

# Fluorescence Sensor Array for Metal Ion Detection Based on Various Coordination Chemistries: General Performance and Potential Application

Zhuo Wang, Manuel A. Palacios, and Pavel Anzenbacher, Jr.\*

Department of Chemistry and Center for Photochemical Sciences, Bowling Green State University, Bowling Green, Ohio 43403

A sensor array containing 9 cross-reactive sensing fluorescent elements with different affinity and selectivity to 10 metal cations ( $\text{Ca}^{2+}$ ,  $\text{Mg}^{2+}$ ,  $\text{Cd}^{2+}$ ,  $\text{Hg}^{2+}$ ,  $\text{Co}^{2+}$ ,  $\text{Zn}^{2+}$ ,  $\text{Cu}^{2+}$ ,  $\text{Ni}^{2+}$ ,  $\text{Al}^{3+}$ ,  $\text{Ga}^{3+}$ ) is described. The discriminatory capacity of the array was tested at different ranges of pH and at different cation concentrations using linear discriminant analysis (LDA). Qualitative identification of cations can be determined with over 96% of accuracy in a concentration range covering 3 orders of a magnitude (5–5000  $\mu\text{M}$ ). Quantitative analysis can be achieved with over 90% accuracy in the concentration range between 10 and 5000  $\mu\text{M}$ . The array performance was also tested in identification of nine different mineral water brands utilizing their various electrolyte compositions and their  $\text{Ca}^{2+}$ ,  $\text{Mg}^{2+}$ , and  $\text{Zn}^{2+}$  levels. LDA cross-validation routine shows 100% correct classification for all trials. Preliminary results suggest that similar arrays could be used in testing of the consistency of the purification and manufacturing process of purified and mineral waters.

The protection and conservation of water resources, preventing contamination from anthropogenic as well as natural sources, is an important effort.<sup>1,2</sup> Among the inorganic contaminants, metal cations play an important role as components of electrolytes and may also present intrinsic risks due to their potential impact on human health and environment.<sup>3–5</sup> For these reasons, improved techniques and alternative technologies to continue improving contaminant detection are widely sought.<sup>6</sup> Here, optical detection,<sup>7</sup> particularly fluorescence methods, shows unique potential for high sensitivity. The power of optical sensors was recently augmented

by implementation of sensor array technologies<sup>8</sup> and pattern recognition methods<sup>9</sup> that allow for identification of multiple metal ions using a single device.<sup>10,11</sup> Even though optical sensors have been widely developed,<sup>12</sup> their integration in a single platform as an array of sensors has been less studied. Most of the recently reported arrays are based on multiple differential binding interactions between a cross-reactive dye indicator and the analyte.<sup>11</sup>

Recently, we have reported a cross-reactive sensor array for metal ions utilizing 8-hydroxyquinoline (8-HQ) coordination chemistry. Such arrays based on fluoro-ionophores bearing just one type of receptor depend mostly on their signal transduction mechanisms to generate discriminatory data.<sup>13</sup> In this study, the cross-reactive sensor array utilizes different kinds of coordination chemistries combined together with different signaling schemes. This approach provides information needed for accurate identification of cations and possibly identification of complex mixtures by their cation content.

## EXPERIMENTAL SECTION

**Chemicals and Solutions.** Commercially available solvents and reagents were used as received from chemical suppliers. Tetrahydrofuran was distilled from a K–Na alloy under argon. All reactions were monitored using Whatman K6F Silica Gel 60

- (8) Schena, M. *Microarray Analysis*; Wiley-Liss: Hoboken, NJ, 2003.
- (9) (a) Albert, K. J.; Lewis, N. S.; Schauer, C. L.; Sotzing, G. A.; Stitzer, S. E.; Vaid, T. P.; Walt, D. R. *Chem. Rev.* **2000**, *100*, 2595–2626. (b) Lavigne, J. J.; Anslyn, E. V. *Angew. Chem., Int. Ed.* **2001**, *40*, 3118. (c) Wright, A. T.; Anslyn, E. V. *Chem. Soc. Rev.* **2006**, *35*, 14–28.
- (10) (a) Garcia-Acosta, B.; Martinez-Manez, R.; Sancenon, F.; Soto, J.; Rurack, K.; Spieles, M.; Garcia-Breijo, E.; Gil, L. *Inorg. Chem.* **2007**, *46*, 3123–3135. (b) Carofiglio, T.; Fregonese, C.; Mohr, G. J.; Rastrelli, F.; Tonellato, U. *Tetrahedron* **2006**, *62*, 1502–1507. (c) Szurdoki, F.; Ren, D.; Walt, D. R. *Anal. Chem.* **2000**, *72*, 5250–5257.
- (11) (a) Basabe-Desmont, L.; Baan, F. van der; Zimmerman, R. S.; Reinhoudt, D. N.; Crego-Calama, M. *Sensors* **2007**, *7*, 1731–1746. (b) Lee, J. W.; Lee, J.-S.; Kang, M.; Su, A. I.; Chang, Y.-T. *Chem. Eur. J.* **2006**, *12*, 5691–5696. (c) Mayr, T.; Igel, C.; Liebsch, G.; Klimant, I.; Wolfbeis, O. S. *Anal. Chem.* **2003**, *75*, 4389–4396. (d) Goodey, A. P.; McDevitt, J. T. *J. Am. Chem. Soc.* **2003**, *125*, 2870–2871. (e) Mayr, T.; Liebsch, G.; Klimant, I.; Wolfbeis, O. S. *Analyst* **2002**, *127*, 201–203.
- (12) (a) McDonagh, C.; Burke, C. S.; MacCraith, B. D. *Chem. Rev.* **2008**, *108*, 400–422. (b) Borisov, S. M.; Wolfbeis, O. S. *Chem. Rev.* **2008**, *108*, 423–461. (c) Buhlmann, P.; Pretsch, E.; Bakker, E. *Chem. Rev.* **1998**, *98*, 1593–1687. (d) de Silva, A. P.; Gunaratne, H. Q.; Gunnlaugsson, T.; Huxley, A. J.; McCoy, C. P.; Rademacher, J. T.; Rice, T. E. *Chem. Rev.* **1997**, *97*, 1515–1566.
- (13) (a) Palacios, M. A.; Wang, Z.; Montes, V. A.; Zyryanov, G. V.; Hausch, B. J.; Jursiková, K.; Anzenbacher, P., Jr. *Chem. Commun.* **2007**, 3708–3710. (b) Palacios, M. A.; Wang, Z.; Montes, V. A.; Zyryanov, G. V.; Anzenbacher, P., Jr. *J. Am. Chem. Soc.* **2008**, *130*, 10307–10314.

\* To whom correspondence should be addressed. E-mail: pavel@bgsu.edu.

- (1) *Heavy Metals in the Environment: Origin, Interaction and Remediation*, 1st ed.; Bradl, H., Ed.; Interface Science and Technology 6; Elsevier: Amsterdam, 2005. (b) Wright, D. A.; Welbourn, P. *Environmental Toxicology*; Cambridge University Press: New York, 2002.
- (2) Marchand, E. A.; Dinkelman, I. *Water Environ. Res.* **2006**, *78*, 1654–1698.
- (3) (a) *Handbook on the Toxicology of Metals*, 3rd ed.; Fowler, B. A., Nordberg, M., Friberg, L., Nordberg, G., Eds.; Academic Press: Boston, MA, 2007. (b) Jaerup, L. *Br. Med. Bul.* **2003**, *68*, 167–182.
- (4) Rasmussen, R. S.; Nettleton, J.; Morrissey, M. T. *J. Aquat. Food Prod. Technol.* **2005**, *14*, 71–100.
- (5) Vahter, M.; Berglund, M.; Akesson, A.; Liden, C. *Environ. Res.* **2002**, *88*, 145–155.
- (6) Barile, F. A. *Principles of Toxicology Testing*; CRC Press: Boca Raton, FL, 2008.
- (7) (a) Borisov, S. M.; Wolfbeis, O. S. *Chem. Rev.* **2008**, *108*, 423–461. (b) Oehme, I.; Wolfbeis, O. S. *Mikrochim. Acta* **1997**, *126*, 177–192.

Å analytical TLC plates by UV detection (254 and 365 nm). Silica gel (60 Å, 32–63 μm) from EMD Science was used for column chromatography. Melting points (uncorrected) were measured using a Thomas-Hoover capillary melting point apparatus. <sup>1</sup>H and <sup>13</sup>C NMR spectra were recorded using either a Varian spectrometer with working frequency 400 MHz or a Bruker instrument (300 MHz). Chemical shifts were referenced to the residual resonance signal of the deuterated solvent. MALDI-TOF-MS were recorded using a Bruker Daltonics Omnicflex spectrometer. **S5** (Lumogallion, TCI) and **S8** (Calcein Blue, TCI) were commercially available from chemical suppliers. **S1**, **S2**, **S3**, and **S4** were synthesized according to procedures published.<sup>14,15</sup> Synthetic procedures for **S6**, **S7**, and **S9** are summarized in Supporting Information (SI).

**Preparation of Submicroliter Sensor Arrays for Cation Sensing.** The sensor materials were prepared by incorporating sensors **S1–S9** into poly(ether)urethane matrixes, which were prepared by casting solutions containing the sensors in a poly(ether)urethane (Tecophilic, SP-93A, Thermedics division from Lubrizol, Cleveland, OH) THF solution (4% w/w) onto a multiwell 10 × 8 (submicroliter) size plate made by ultrasonic drilling. The concentrations of sensors **S1–S9** in THF vary (**S1** 1 mM, **S2** 1 mM, **S3** 1 mM, **S4** 1 mM, **S5** 0.5 mM, **S6** 0.1 mM, **S7** 1 mM, **S8** 0.5 mM, **S9** 1 mM). The chloride salts of the cations were administered as aqueous solutions. In order to evaluate responses of different cations at different pHs, the concentration of cation solution was 1 mM. pH was adjusted in solution by addition of NaOH (0.01 M) or HCl (0.01 M) utilizing a Titrator T50 (Mettler Toledo Co.) with an accuracy of pH ± 0.1 and the solutions were used immediately after preparation. Mineral water analysis was carried out by applying 200 nL (directly from the bottle) to the array elements.

**Fluorescence Sensor Array Image Acquisition and Data Processing.** Images from the sensor arrays are recorded using a Kodak Image Station 440CF. The scanned images (12 bit) are acquired with a resolution of 433 × 441 pixels/in. and with gray levels over 1000 (12-s exposures). The sensor arrays are excited with a broadband UV lamp (300–400 nm, λ<sub>max</sub> = 330 and 365 nm), and up to four channels are used for emission detection: (1) blue, band-pass filter 380–500 nm λ<sub>max</sub> = 435 nm; (2) green, band-pass filter 480–600 nm λ<sub>max</sub> = 525 nm; (3) yellow, long-pass filter 523 nm; (4) red, long-pass filter 580 nm.<sup>16</sup> The false color images were obtained by recording the BW images using blue, green, and red filters. These images were then merged in equal proportion using NIH ImageJ software.<sup>17</sup> The RGB triplet corresponds with the color of the filter used. After acquiring the images, the integrated (nonzero) gray pixel (*n*) value is calculated for each well of each channel. Images of the sensor chip were recorded before (*b*) and after (*a*) the addition of an analyte, and their final normalized responses (*R*) were evaluated as follows:

$$R = \sum_n \frac{a_n}{b_n} - 1 \quad (1)$$

**Data Analysis.** In this study, we used linear discriminant analysis (LDA), as it yielded better results compared to unsupervised methods such as principal component analysis and hierarchical clustering analysis.<sup>18</sup> LDA is a classical statistical approach for supervised dimensionality reduction. Using the defined group classes, it aims to maximize the ratio of the between-class distance to the within-class distance, thus maximizing the class discrimination. LDA was used in a complete way considering all 36 variables (9 sensors, 4 channels RGBY). A cross-validation routine was implemented in order to compensate for the bias imposed when a sample classification is attempted while using a training set that contains the same sample. The cross-validation (leave-one-out) routine is used to test the predictability of the sensor array by leaving one observation out of the set at the time and uses the rest of the data as a training set to generate the linear discriminant function. The LD function is then used for the classification of the excluded observation. This is performed for each observation, and the overall ability to classify the observations describes the quality and predictability of the array. The implementation of LDA is rather conveniently used for determination of classes by using the LD discriminant function and also provides a graphical output by plotting discriminant scores against the canonical roots. These plots provide a graphical representation of how LDA is clustering similar patterns, and it attests to the degree of discrimination of the data, i.e., how good the resolution of the array is for a given group of samples.

## RESULTS AND DISCUSSION

**Selection of Chemosensors.** The criteria for the selection of chemosensors (fluoro-ionophores) were guided by the following requirements: The coordination chemistry of the chemosensor should allow for significant cross-reactivity (i.e., selective chemosensors were not particularly sought). The chemosensors should have strong absorption in the near-UV (300–400 nm), for which the LED light sources are widely available, as well as reasonably strong emission in the visible region. Also, the chemosensors should be commercially available or easy to synthesize. In general, it is desirable to generate a maximum discriminatory power with a minimal set of sensors. Guided by the above criteria, we have selected a set of nine chemosensors (**S1–S9**) (Figure 1) to generate the array capable of analyte differentiation based on a metal ion content. Chemosensors **S1–S9** comprise different kinds of receptors as well as different kinds of signal transduction schemes. Therefore, it is the combination of different coordination chemistries and signal transduction schemes, such as fluorescent enhancement or quenching and ratiometric response, that generates enough discriminatory data for accurate classification of possible analytes, while keeping the number of sensing elements as low as possible. Here, the **S1** and **S2** were chosen based on our previous attempts to generate cross-reactive cation sensors.<sup>13</sup> **S1** and **S2** comprise the same 8-HQ receptor and different

(14) Sensors **1** and **2**: (a) Montes, V. A.; Pohl, R.; Shinar, J.; Anzenbacher, P., Jr. *J. Org. Chem.* **2004**, *69*, 1723–1725. (b) Montes, V. A.; Pohl, R.; Shinar, J.; Anzenbacher, P., Jr. *Chem.-Eur. J.* **2006**, *12*, 4523–4535.

(15) (a) Sensor **3**: Macias, B.; Garcia, I.; Villa, M. V.; Borrás, J.; Castineiras, A.; Sanz, F. *Polyhedron* **2002**, *21*, 1229–1234. (b) Sensor **4**: Bag, B.; Bharadwaj, K. *J. Phys. Chem. B* **2005**, *109*, 4377–4390.

(16) The use of the optical filters may be circumvented by using a sensitive 36-bit color camera. This way, the detection setup could be simplified and rendered more practicable.

(17) Rasband, W. S.; Image J. U. S. National Institutes of Health, Bethesda, MD, <http://rsb.info.nih.gov/ij/>, 1997–2008.

(18) (a) Beebe, K. R.; Pell, R. J.; Seasholtz, M. B. *Chemometrics: a practical guide*; Wiley: New York, 1998. (b) Otto, M. *Chemometrics: Statistics and computer application in analytical chemistry*; Wiley-VCH: Weinheim, 1999. (c) Jambu, M. *Exploratory and Multivariate Data Analysis*; Academic Press: Boston, 1991.

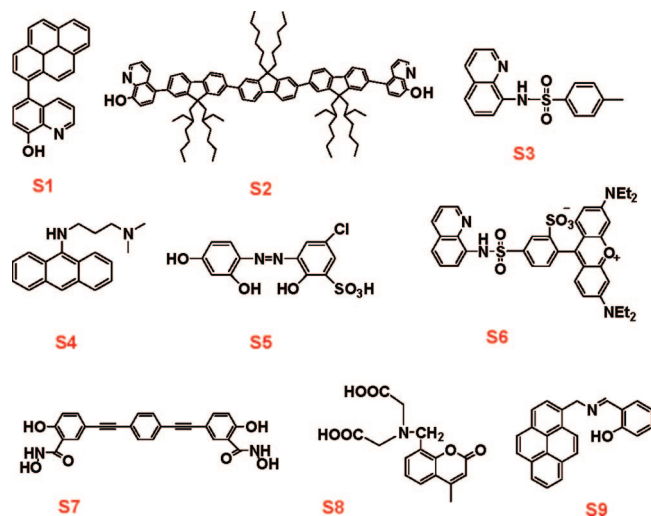


**Figure 1.** Structure of chemosensors **S1–S9** used in the array.

conjugated chromophores to yield a different response to various metal cations. This is because the conjugated chromophores attached to the receptor are partially quenched in their resting state, and upon the cation coordination by the 8-HQ, the resulting metalloquinolinolate complex displays a change in fluorescence. The nature of the changes in the fluorescence is highly dependent on the cation. Sensors **S3** and **S4** have been reported in the literature, and their properties have been studied.<sup>15,19,20</sup> Sensors **S6**, **S7**, and **S9** have for the first time been synthesized for the purpose of this study; however, the coordination chemistry of similar compounds has been previously characterized in literature.<sup>21</sup> The coordination chemistry of **S6** is similar to that of **S3**, although the signal transduction in **S6** and **S7** is based on fluorescence quenching rather than its enhancement, while **S9** displays a fluorescence turn-on behavior. Finally, **S5** (Lumogallion) and **S8** (Calcein Blue) are commercially available, and their sensing properties have been characterized.<sup>22</sup> The relative binding affinities for the chemosensors **S1–S9** and cations of this study are shown in the SI. Finally, incorporating a chemosensor with different optical transduction schemes (turn-on, turn-off, and ratiometric) is likely to result in an expanded response variance space. In case a metal ion can induce a variety of responses (turn-on, turn-off, and ratiometric), then the increments to the variance within the  $n$ -dimensional vector response generated by the array for that given metal ion are also likely to increase. Thus, more information could be generated and the discriminatory power of the array would be enhanced.

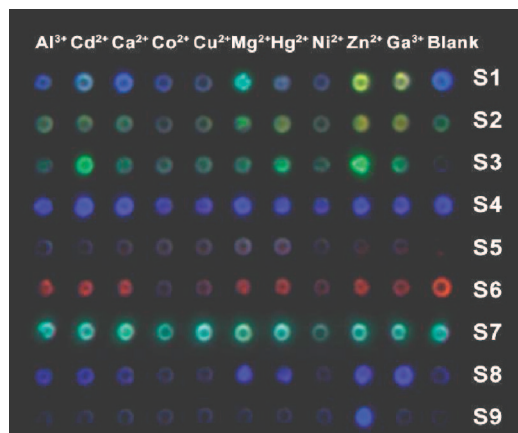


**Figure 2.** Fluorescence responses of the **S1–S9** sensor array to the presence of different cations (1 mM in water, 200 nL, pH 7). False color representation generated by superimposing of the equally weighed images corresponding to RGB channels.

### Configuration of the Array and Optical Sensor Membranes.

The solid-state array was fabricated as reported previously using sensors **S1–S9** dispersed in a hydrophilic polyurethane carrier (~0.07% **S1–S9** in polyurethane, w/w) to yield a simple two-component optode. The purpose of the hydrophilic polyurethane is to draw in water while coextracting the metal ions and counterions, thus aiding in the formation of the metal–sensor complexes, and to overcome the incompatibility in solubility of the lipophilic sensors and hydrophilic cations. The 200 nL of a THF solution containing a sensor and polymer is then cast into the wells of a multiwell 9 × 8 (submicroliter) size plate to yield ~10- $\mu$ m-thick membranes in each well.

The luminescence output from the array was recorded using four detection channels corresponding to the blue, green, yellow, and red region of the visible spectrum. Upon addition of the aqueous cation solutions to the wells, the emission of the array was rerecorded. The metal ions tested were  $\text{Al}^{3+}$ ,  $\text{Cd}^{2+}$ ,  $\text{Ca}^{2+}$ ,  $\text{Co}^{2+}$ ,  $\text{Cu}^{2+}$ ,  $\text{Mg}^{2+}$ ,  $\text{Hg}^{2+}$ ,  $\text{Ni}^{2+}$ ,  $\text{Zn}^{2+}$ , and  $\text{Ga}^{3+}$  in the form of their chloride salts in water (1 mM in water, 200 nL, pH 7) (Figure 2). Figure 2 shows a false color representation of the changes in the sensor array induced by the metal ions. A quick inspection reveals distinctive response patterns generated for each of the cations tested. Above all,  $\text{Zn}^{2+}$  is an ion that presents the most distinct response pattern due to, among others, the high selectivity of **S9** for this ion.

In order to quantify the changes in luminescence, the nonzero pixels were integrated for each well. As predicted, each of the metal cations induced analyte-specific changes in luminescence in the individual chemosensors of the array, thus creating a multidimensional response pattern (Figure 3, left). Figure 3 shows several examples of the response pattern generated by the sensor array in the presence of  $\text{Mg}^{2+}$ ,  $\text{Cu}^{2+}$ , and  $\text{Zn}^{2+}$ . Inspection of the emission patterns reveals that **S8** is the most sensitive sensor for  $\text{Mg}^{2+}$ , while **S6** is for  $\text{Cu}^{2+}$  and **S3** for  $\text{Zn}^{2+}$ . Supporting Information shows the response patterns for all of the metal cations and all sensors at three different pHs (5, 6, 7). The multidimensional response patterns (36-dimensional, 9 sensors × 4 RGBY channels) of the sensor array in the presence of 10 cations ( $\text{Ca}^{2+}$ ,  $\text{Mg}^{2+}$ ,  $\text{Cd}^{2+}$ ,  $\text{Hg}^{2+}$ ,  $\text{Co}^{2+}$ ,  $\text{Zn}^{2+}$ ,  $\text{Cu}^{2+}$ ,  $\text{Ni}^{2+}$ ,  $\text{Al}^{3+}$ ,  $\text{Ga}^{3+}$ ) were further studied using LDA.<sup>18</sup>

- (19) (a) Nowicki, J. L.; Johnson, K. S.; Coale, K. H.; Elrod, V. A.; Lleberrmad, S. H. *Anal. Chem.* **1994**, *66*, 2732–2138. (b) Prat, M. D.; Guiteras, J.; Compano, R.; Beltran, J. L. *J. Fluoresc.* **1991**, *1*, 267–272.
- (20) Bag, B.; Bharadwaj, P. K. *J. Phys. Chem. B* **2005**, *109*, 4377–4390.
- (21) (a) O'Brien, E. C.; Roy, S. L.; Levaillain, J.; Fitzgerald, D. J.; Nolan, K. B. *Inorg. Chim. Acta* **1997**, *266*, 117–120. (b) Garcia, B.; Gonzalez, S.; Hoyuelos, F. J.; Ibeas, S.; Leal, J. M.; Senent, M. L.; Biver, T.; Secco, F.; Venturini, M. *Inorg. Chem.* **2007**, *46*, 3680–3687. (c) Abe, A. M. M.; Helaja, J.; Koskinen, A. M. P. *Org. Lett.* **2006**, *8*, 4537–4540.
- (22) (a) Carroll, M. K.; Bright, F. V.; Hieftje, G. M. *Anal. Chem.* **1989**, *61*, 1768–1772. (b) Du, M.; Huie, C. W. *Anal. Chim. Acta* **2001**, *443*, 269–276. (c) Suthermer, S. H.; Cabaniss, S. E. *Anal. Chim. Acta* **1995**, *303*, 211–221. (d) Royzen, M.; Dai, Z.; Canary, J. W. *J. Am. Chem. Soc.* **2005**, *127*, 1612–1613. (e) West, T. S. *Anal. Chim. Acta* **1961**, *25*, 301–307. (f) Gee, K. R.; Zhou, Z.-L.; Ton-That, D.; Sensi, S. L.; Weiss, J. H. *Cell Calcium* **2002**, *31*, 245–250.

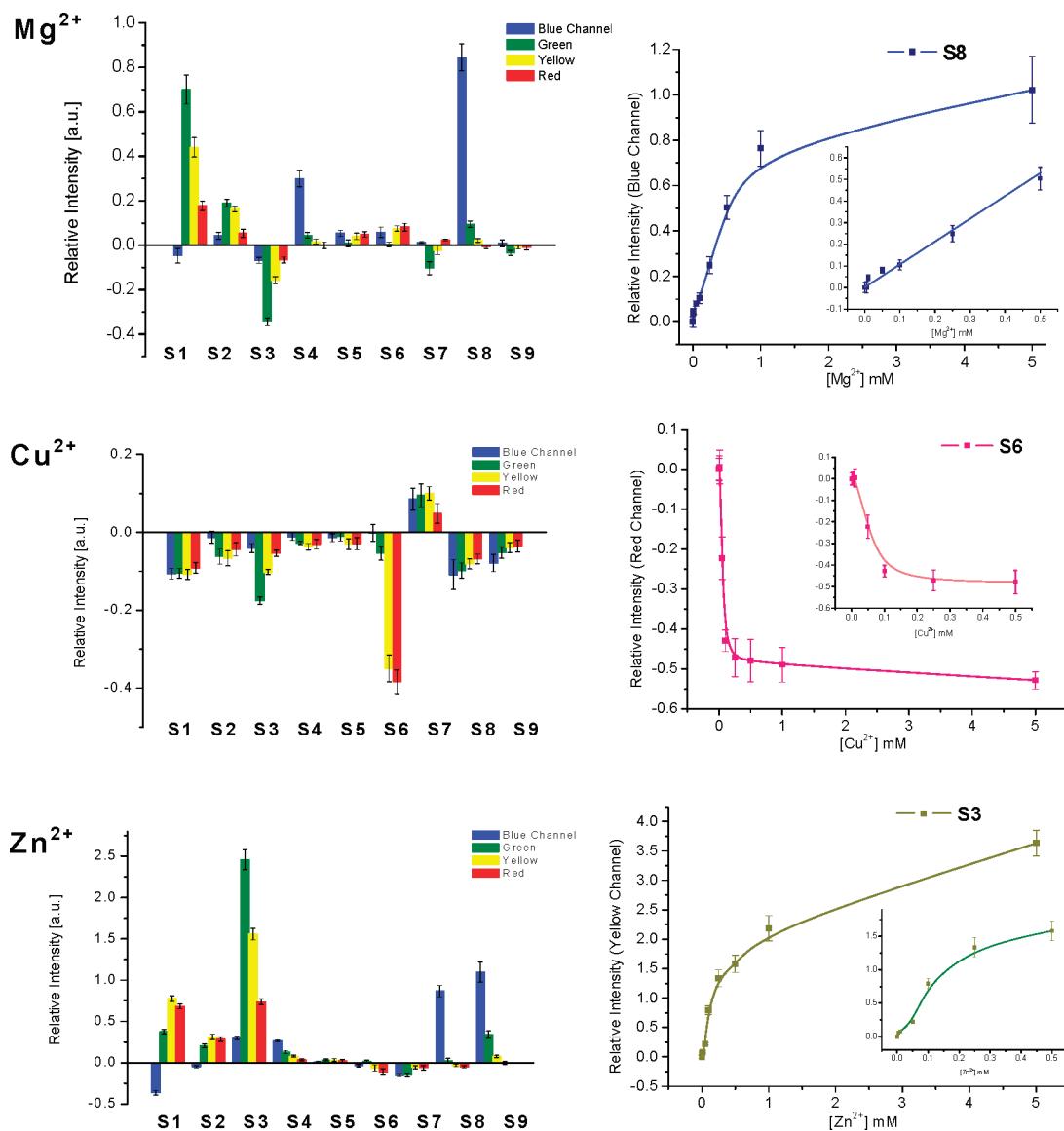


**Figure 3.** Left: Response patterns (**S1**–**S9**, raw data) to aqueous  $\text{Mg}^{2+}$ ,  $\text{Cu}^{2+}$ , and  $\text{Zn}^{2+}$  solutions (200 nL, 1 mM, pH 7). Right: Changes of the relative intensity of **S8** (blue channel), **S6** (red channel), and **S3** (yellow channel) with increasing ion concentrations. Inset: Detail of a low concentration (0–500  $\mu\text{M}$ ) region.

Furthermore, Figure 3, right panel, shows examples of quantitative representation of changes in the relative intensity of **S8** (blue channel) in the presence of  $\text{Mg}^{2+}$ , **S6** (red channel) in the presence of  $\text{Cu}^{2+}$ , and **S3** (yellow channel) in the presence of  $\text{Zn}^{2+}$  at different concentrations of ions ranging from 5  $\mu\text{M}$  to 5 mM. The individual dynamic ranges of the sensing elements differ for each cation. Thus, for the sensor array **S1**–**S9**, we have identified the lower and upper limits of quantification given by the chemosensors capable of addressing the lowest and highest concentrations. For example, the dynamic range of the array for  $\text{Mg}^{2+}$  is defined to be between 20 (defined by **S1**) and 2000  $\mu\text{M}$  (defined by **S8**).<sup>23</sup>

**Effect of pH on the Sensor Array Response.** In the situation where the sensors comprise potentially pH-sensitive chemical moieties, it is necessary to study the possible effect of water (blank) solutions at different pH on the overall response of the array. Therefore, we first studied the changes in the array fluorescence at a range of pH from 1 to 14 and applied LDA to

the data generated as a response of the array to varying pH (Figure 4). LDA generates a new space defined by the canonical roots (factors or discriminant axes) to provide the best description of similarities and differences between samples. Each pattern generated by the sensor array can be reduced to a single score and plotted in the new canonical space (canonical score plot). Relative distances between the scores in the canonical space can be correlated with similarities or difference in the responses generated by the samples. From the canonical score plot, one can see that the responses could be divided into four clusters. The first cluster includes pH 1–4, a second cluster that includes the pH range 5–7, and the third cluster corresponding to pH 8–13. The fourth cluster then corresponds to pH of 14. The third cluster appears to cover a larger area of the canonical space, presumably due to the varying deprotonation processes taking place in different chemosensors in the pH range between 8 and 13.

Because of the potential applications, we decided to work in the pH region between 5 and 7, which is more appealing for

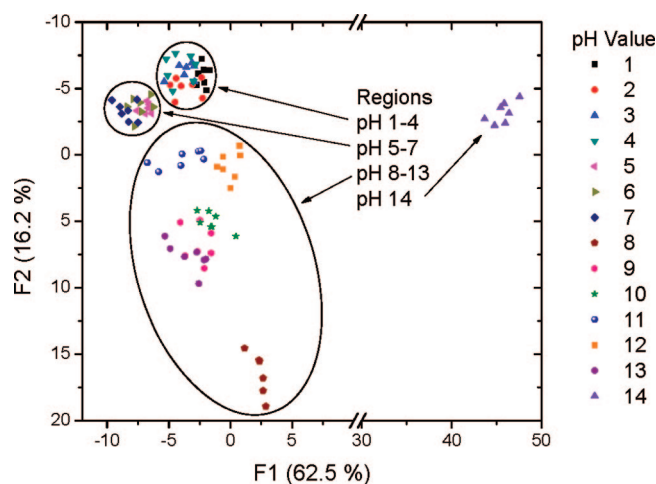


**Figure 4.** LDA canonical score plot for the response of the array to blanks at different pH levels.

potential biological and environmental applications. In this pH range, the response of the array does not show significant differences in response, presumably due to the cation coordination chemistry of the receptors within this pH range. Also, at low pH (pH <4), protonation of the coordination sites of the receptors can affect the photophysical and coordination chemistry properties of the chemosensors. On the other hand, at high pH (pH >8), the receptor deprotonation might affect the chemosensor properties, and the solubility of the metal salts/hydroxides decreases. Hence, we decided to evaluate the array performance in cation classification within the pH “comfort zone” at three different pH levels: 5, 6, and 7. At pH 5, 6, and 7, all metal salts are soluble at concentrations of  $\leq 2$  mM. The cations affected by pH are  $\text{Al}^{3+}$  or  $\text{Cu}^{2+}$ , albeit only at high concentrations. Due to high sensor–cation affinities, sensors **S1–S9** show saturation at 1 mM (Figure 3 and SI). Thus, the lower solubility of metal salts at pH 7 does not appreciably affect the analyses. For each pH, a data set corresponding to 10 cations (8 trials) was generated. LDA was first applied separately to each data set (Figure 5). Figure 5 shows LDA canonical score plots for the first 3 factors (10 different metal ions) at three different pH conditions. Three factors were necessary to describe at least 85% of the total information (variance) contained in the data set. Here, the cross-validation routine shows 100% accuracy for the classification of all cations at all three pH levels. Even though the pH does not seem to have a significant effect on the predictability of the overall array behavior, the individual cations show a major difference between the pH levels.

In order to determine whether the data obtained using 10 cations at three different pHs could be used for cation determination at a particular pH or for pH-independent cation detection within the range of pH (5–7), a LDA was carried out including all 240 trials. First, LDA was used to investigate the data describing the array response to cations at a particular pH as a grouping variable to study the ability of the array to distinguish the 30 classes (10 metal ions  $\times$  3 pHs). LDA cross-validated (leave-one-out) classification shows 99% accuracy for all 10 cations at pHs 5, 6, and 7. This result is remarkable given the fact that some cations, such as  $\text{Cd}^{2+}$ , present a very similar response profile at different pHs (Figure 6, left). Second, LDA was used to investigate the data set in which the cation class is used as a grouping variable (Figure

6, right) to test if regardless of the pH (5, 6, or 7) the LDA can accurately identify the metal ion. Here, the LDA shows 97% accurate classification, thus showing that the accurate pH-independent classification of the cation can be predicted even though there are cations such as  $\text{Al}^{3+}$  and  $\text{Zn}^{2+}$  that yield very different response patterns at each pH.

**Array Performance at pH 7.** The limit of a detection concept in arrays can be translated into the limit of discrimination, i.e., the concentration at which the sensor array is capable of discriminating between different analytes. Therefore, we studied the array performance at various concentration ranges. For this reason, a data set comprising 10 cations at 8 different concentrations (5–5000  $\mu\text{M}$ , 8 trials each) at pH 7 was generated. LDA was applied to all 640 trials using cation concentration or cation class as a grouping variable (Table 1). First, the cation class is used as a grouping variable to test if regardless of the concentration it is possible to qualitatively identify the cations. As seen in Table 1, LDA cross-validation routine shows overall 96% of correct classification. The accuracy of the classification differs for each cation. For example, 88% classification accuracy was observed for  $\text{Cu}^{2+}$  and 100% for  $\text{Zn}^{2+}$ . This behavior correlates with dynamic ranges of the different sensing elements for different cations. For example, in the case of  $\text{Cu}^{2+}$ , the overall dynamic range of the array lies between 20 and 500  $\mu\text{M}$ , while for  $\text{Zn}^{2+}$  the overall dynamic range is  $\sim 5$ –5000  $\mu\text{M}$ .<sup>24</sup> Thus, it was necessary to evaluate the dependence of the discriminatory capacity of the array at different dynamic ranges (Table 1:  $\geq 5$   $\mu\text{M}$ , 5–5000  $\mu\text{M}$ ;  $\geq 10$   $\mu\text{M}$ , 10–5000  $\mu\text{M}$ ;  $\geq 50$   $\mu\text{M}$ , 50–5000  $\mu\text{M}$ ; and  $\geq 100$   $\mu\text{M}$ , 100–5000  $\mu\text{M}$ ). The classification accuracy data corresponding to these four dynamic ranges are listed in Table 1. The discriminatory capacity for cation identification exceeds 95% overall accuracy at  $\sim 5$   $\mu\text{M}$  and 99% overall accuracy at the concentration  $\geq 50$   $\mu\text{M}$ .

On the other hand, when the cation concentration is used as a grouping variable instead of the cation class, the analysis will allow for determining the array’s capability to discriminate between 80 groups of analytes (10 cations  $\times$  8 concentrations) and perform a quantitative analysis.

Even though LDA is not a regression technique, it can be used to plot the concentration response dependence (trajectory) in the LDA canonical space (Figure 7). Figure 7 shows trajectories composed of the average scores for each concentration of a given cation. From the discriminant score plots it is clear that at lower concentration (close to the origin of the plots) it is harder to discriminate between different cations in different concentrations. In the case of quantitative determination of cations, the limit of discrimination depends even more on the overall dynamic range of the sensor array. This is because not only are the general trends in the response pattern (within a class of cation) important but mostly the magnitude (of the change in the response) in these trends affects the assignment/interpretation of the concentration by the array. This implies that all of the patterns will tend to be more similar at a low concentration where the sensors are close to their LODs.

(23) Concentrations of heavy metals exceeding 5  $\mu\text{M}$  are, perhaps, too high for a number of practical applications. The current high LOD could be circumvented by preconcentration of the analyte. This is particularly feasible due to the small amount of a sample needed for the test ( $\sim 2$   $\mu\text{L}$  per replica).

(24) See Supporting Information.

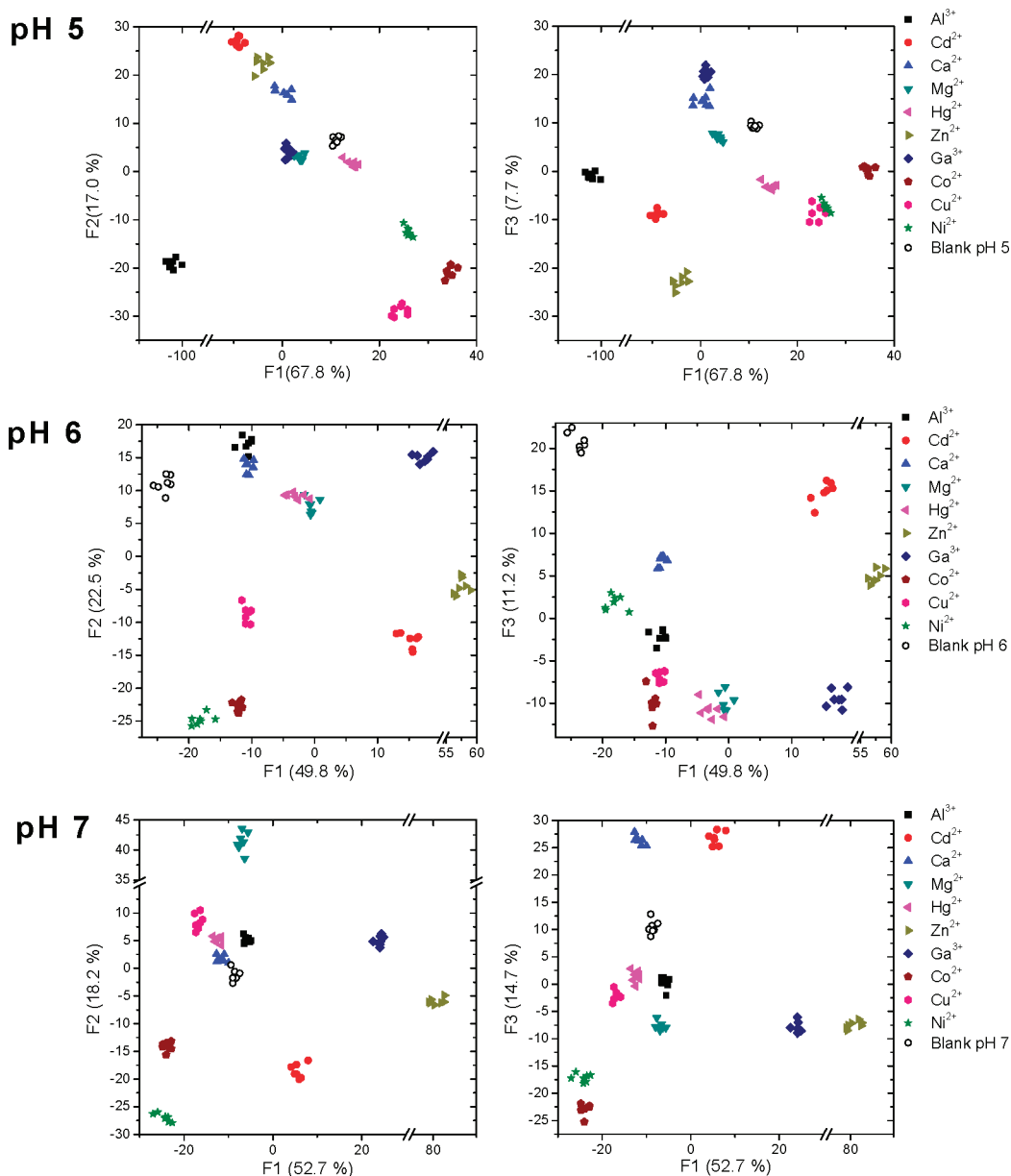


**Figure 5.** LDA canonical score plots describing the response of the **S1–S9** array to 10 cations (1 mM) at three different pHs (5, 6, 7). Three factors were necessary to describe at least 85% of the total information (variance) contained in the data set. Data sets (10 cations + blank, 8 trials) recorded at different pH levels were evaluated. For each pH, the cross-validation routine shows 100% correct classification.

As in the case of qualitative determination of cations, we applied LDA to the array response at different concentrations and calculated the percentages for the correct classification of cation concentration (Table 1). LDA using a cross-validation routine shows 85% classification accuracy at a threshold of 5  $\mu\text{M}$ . Here, the misclassified data correspond to the 15%, corresponding to 97 trials out of 648 trials. Interestingly, just one trial was misclassified as another cation ( $\text{Cu}^{2+}$  5  $\mu\text{M}$  misclassified as  $\text{Al}^{3+}$  5  $\mu\text{M}$ ); the remaining 96 trials were classified as a correct cation, but at incorrect concentration. For example, a  $\text{Ni}^{2+}$  5  $\mu\text{M}$  trial was misclassified as  $\text{Ni}^{2+}$  10  $\mu\text{M}$ ,  $\text{Al}^{3+}$  1000  $\mu\text{M}$  was misclassified as  $\text{Al}^{3+}$  5000  $\mu\text{M}$ , etc. Also, 38 misclassifications are evenly distributed between  $\text{Cu}^{2+}$  and  $\text{Hg}^{2+}$  ions. This is because the sensors **S1–S9** show a similarly limited dynamic range between 20 and 500  $\mu\text{M}$  for these two cations. Thus, 13 out of 22 misclassifications for  $\text{Cu}^{2+}$  are between 5 and 10

$\mu\text{M}$ , and 9 out of 21 misclassifications for  $\text{Hg}^{2+}$  appear in the same concentration range.

At the concentration range of 10–5000  $\mu\text{M}$ , where the cation concentrations are out of the LOD zone for most of the sensor elements, the accuracy of the concentration prediction increases to 91%. The same trend is observed with the concentration increased to 50 and 100  $\mu\text{M}$  corresponding to the overall classification accuracy of 93 and 95%, respectively. In contrast, the correct quantitative determination of  $\text{Ni}^{2+}$  and  $\text{Cu}^{2+}$  seemed to decrease at the concentration range of 50–5000  $\mu\text{M}$  and higher, presumably due to the fact that most sensors display saturation at  $\sim 1$  mM for these two cations. However, the **S1–S9** array still shows a limit of discrimination of 10  $\mu\text{M}$  for quantitative determination of the cation concentration with more than 90% of classification accuracy, while for qualitative determination, the limit of discrimination is 5  $\mu\text{M}$ .

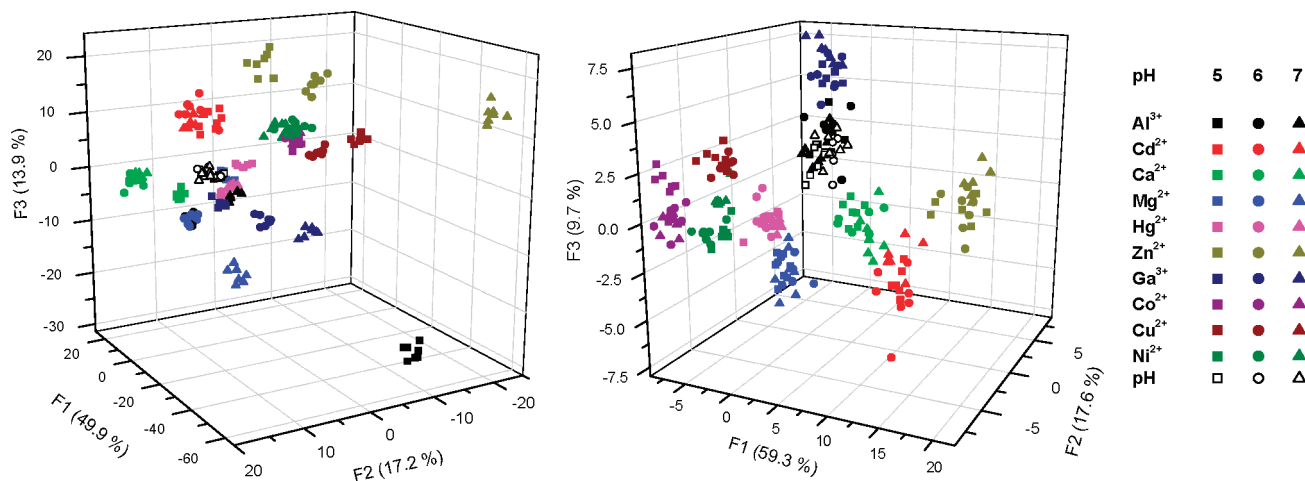


**Figure 6.** LDA canonical score plots for the response of the **S1–S9** array to 10 cations (1 mM) at three different different pH levels (5, 6, 7). Left: LDA was performed using “M<sup>n+</sup> at pH X” as a grouping variable. Right: LDA performed using only the cation class as a grouping variable.

**Table 1. LDA Cross-Validated (Leave-One-Out) Classification Accuracy for 10 Different Metal Ions at Different Dynamic Ranges of Concentration<sup>a</sup>**

concentration threshold	correct proportion for prediction of metal ion class				correct proportion for prediction of metal ion concentration			
	≥5 μM	≥10 μM	≥50 μM	≥100 μM	≥5 μM	≥10 μM	≥50 μM	≥100 μM
classification	0.96	0.97	0.99	0.99	0.85	0.91	0.93	0.95
blank (pH 7)	1.00	1.00	1.00	1.00	1.00	1.00	1.00	1.00
Al <sup>3+</sup>	0.97	0.98	1.00	1.00	0.83	0.86	0.90	0.90
Ca <sup>2+</sup>	0.95	1.00	1.00	1.00	0.79	0.82	0.86	0.98
Cd <sup>2+</sup>	1.00	0.98	1.00	1.00	0.89	1.00	1.00	1.00
Co <sup>2+</sup>	1.00	1.00	1.00	1.00	0.92	0.97	0.98	0.98
Cu <sup>2+</sup>	0.88	0.89	0.96	1.00	0.67	0.84	0.81	0.78
Ga <sup>3+</sup>	0.91	0.88	1.00	1.00	0.91	0.95	0.94	0.93
Hg <sup>2+</sup>	0.94	0.96	0.96	1.00	0.66	0.70	0.82	0.93
Mg <sup>2+</sup>	0.94	0.94	0.94	0.98	0.89	0.89	0.96	1.00
Ni <sup>2+</sup>	1.00	1.00	1.00	1.00	0.89	0.98	0.96	0.93
Zn <sup>2+</sup>	1.00	1.00	1.00	1.00	0.97	1.00	1.00	1.00

<sup>a</sup> Upper limit is 5 mM, in all cases.

Within the training sets defined by a cation type, concentration, and pH, the array performance is very good (in most cases >95% correct classification) considering that it consists of only nine sensor elements. This is due to the known and predictable coordination chemistry of the receptors and the luminescence signaling displayed by these sensors, which is different from previous contributions.<sup>11</sup> The chemosensors used in this work are cross-reactive but maintain certain predictable selectivity in binding while the fluorescence signaling, which is individual for each probe and cation, seems to add yet another layer of information utilized in the analysis. Taken in concert, the intrinsic binding profiles and fluorescence signaling features generate enough discriminatory data to distinguish among 10 cations in a wide range of concentrations. This supports the hypothesis that cross-reactive, yet selective sensing elements might help by increasing the response space and as a consequence the discriminatory power of sensor arrays.<sup>13b,25</sup> While these results reported here appear to be promising, it should be noted that the performance and practicability of the array are limited to the generated training sets. Nonetheless, we believe that this kind of sensor arrays could, perhaps, be utilized in multi-ion detection schemes, particularly if aided by advanced classification algo-

rithms, such as support vector machines or artificial neural networks.<sup>18</sup>

**Mineral Water Brand Identification Based on Metal Ion Content.** Encouraged by the latest results, we decided to explore the utility of the **S1–S9** sensor array by exploring a potential application: identification of mineral and purified (Aquafina) waters based on their cation content (mostly Ca<sup>2+</sup>, Mg<sup>2+</sup>). For mineral water analysis, the responses for nine commercial brands along with two controls/blanks (Nanopure water and tap water) were collected. Figure 8 lists the calcium and magnesium ion contents for all of the mineral water brands. The pH levels of all these brands are in the range of 5–7 where the sensor array presents a rather flat response. From the list (Figure 8) it is clear that all eight brands contain different kinds and concentrations of cations and also in different proportions. Furthermore, from the range of cation concentrations and their kinds, it could be expected that our sensor array could generate a fingerprint-like response pattern for each brand of water based on their cation content.<sup>26</sup> Cross-validation routine shows 100% correct classification for all 88 trials (Figure 8, right). Interestingly, Aquafina brand, due to its low electrolyte content, presents a very weak response owing to the fact that it is closest to the Nanopure water by cation content;



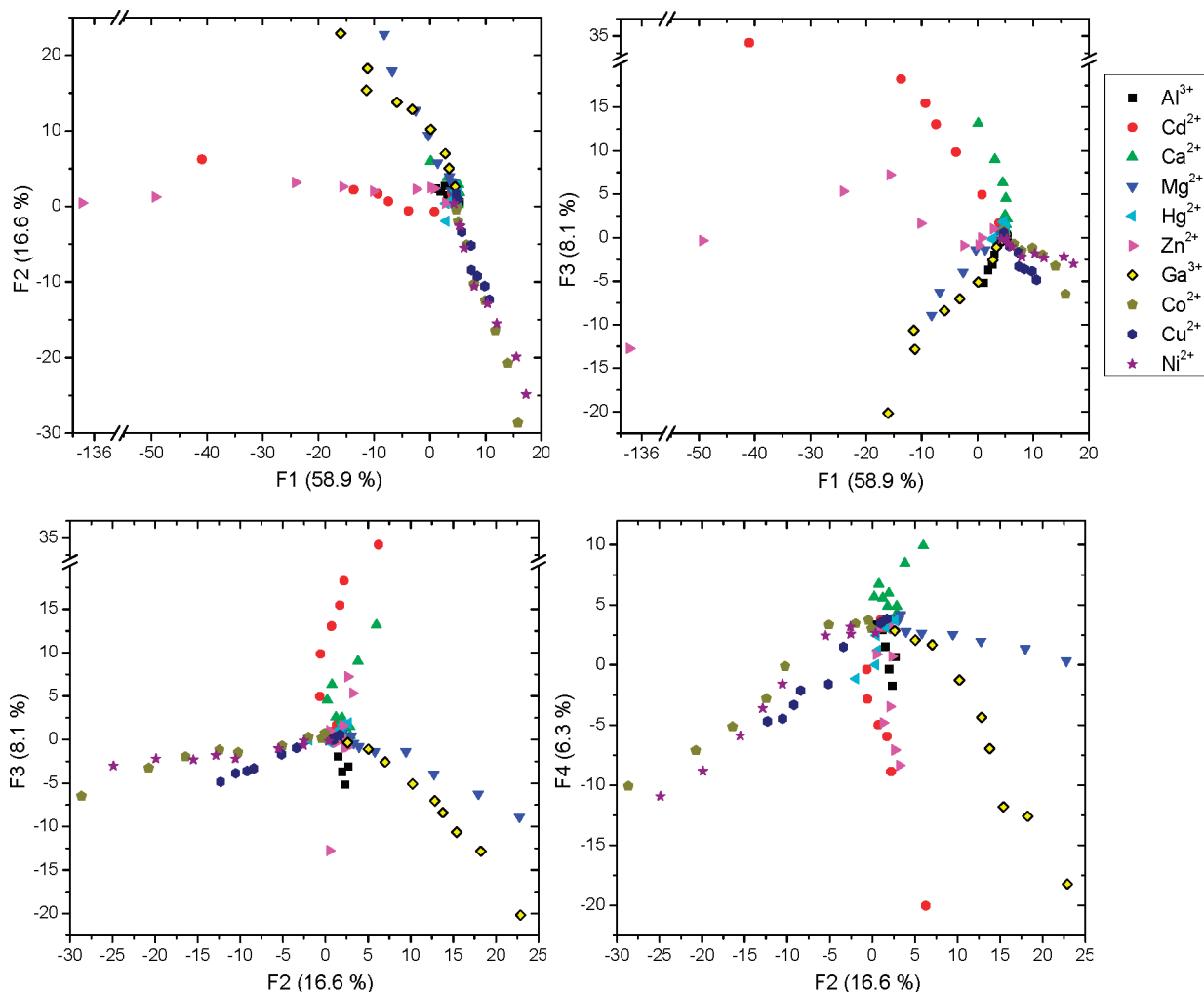


**Figure 7.** LDA canonical score plots describing the response of the **S1–S9** array to 10 different metal ions at a concentration range between 5 and 5000  $\mu\text{M}$ . Concentration trajectories are derived from/calculated as the average of the scores for each concentration of a given cation.

Mineral Water	Metal Ion Content (mg/L)				pH
	Ca <sup>2+</sup>	Mg <sup>2+</sup>	Na <sup>+</sup>	K <sup>+</sup>	
Aquafina	~0	~0	~0	~0	7.1
Biovive	42	3.8	2.5	0.6	7.5
Bonaqua	62	41	118	10.8	6.1
Evian	78	24	5	1	7.3
Fiji	17	13	17	1	7.5
Gerolsteiner	348	108	118	10.8	6.6
Magnesia	38	234	5	1	7.0
Naleczowianka	114	23	13	5	7.5
Perrier	149	7	12	1	5.1

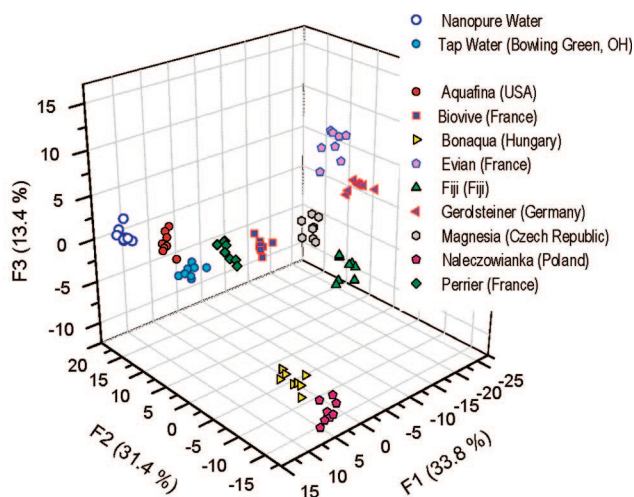


**Figure 8.** Left: Metal ion content for different brands of mineral and purified water samples. Right: LDA canonical score plots corresponding to the response of the **S1–S9** array to 9 different water brands. The data set contains 9 brands and 2 blanks, 8 trials each. LDA shows 100% correct classification for all water brands.

Aquafina is actually not commercialized as a “mineral water”, but as “pure water”.

As a control experiment, we have tried to determine the consistency in the cationic fingerprint of mineral water Evian.<sup>27</sup>

For this brand, three different bottles from different lots were selected randomly and tested using the **S1–S9** sensor array. The responses were recorded and evaluated in the discriminant function generated from the analysis of the mineral waters. LDA

classified the three Evian bottles as Evian (100% correct classification).

## CONCLUSION

A sensor array containing nine selective, yet cross-reactive, sensing elements has been presented. The interplay between the selectivity and cross-reactivity given by a different kind of cation–receptor coordination chemistry along with different signaling schemes was successfully exploited/utilized to provide highly cross-reactive and provide an information-rich fluorescence output in four (RGBY) emission channels. This easy-to-observe luminescence output may be used for both qualitative and quantitative analyses of metal ions. A pattern recognition method (LDA) was used to evaluate the analytical utility of the described sensors in the array. The discriminatory capacity of the array was tested using a set of 10 metal ions at different ranges of pH and at different concentrations. Qualitative identification of cations can be determined with over 96% of accuracy in a concentration range covering 3 orders of a magnitude (5–5000  $\mu\text{M}$ ). Quantitative analysis can be achieved with over 90% accuracy in the concentration range between 10 and 5000  $\mu\text{M}$ .

The discriminatory capacity of the described sensors and arrays was also tested in identification of nine different mineral

---

(25) (a) Palacios, M. A.; Nishiyabu, R.; Marquez, M.; Anzenbacher, P., Jr. *J. Am. Chem. Soc.* **2007**, *129*, 7538–7544. (b) Zyryanov, G. V.; Palacios, M.; Anzenbacher, P., Jr. *Angew. Chem., Int. Ed.* **2007**, *119*, 7995–7998.

(26) The electrolyte contents of the water samples are listed in the Supporting Information.

(27) Evian was selected for the ease in finding different production lots.

water brands utilizing their various electrolyte compositions and their  $\text{Ca}^{2+}$ ,  $\text{Mg}^{2+}$ , and  $\text{Zn}^{2+}$  levels. The present sensor array is capable of discriminating among these complex analytes that were used without any pretreatment (directly from the bottle). Preliminary results suggest that similar arrays could be used in testing of the consistency of the purification or manufacturing process of purified and mineral waters. Finally, we believe that this kind of sensor array could be further exploited for application in multi-ion detection schemes by implementing more advanced classification algorithms, such as support vector machines or artificial neural networks, which is a subject of our continuing efforts.

## ACKNOWLEDGMENT

P.A. gratefully acknowledges support from the Alfred P. Sloan Foundation, BGSU (Technology Innovations Enhancement grant), and the NSF (CHE 0750303, SENSOR 0330267). M.A.P. acknowledges the support from the McMaster Endowment for a fellowship.

## SUPPORTING INFORMATION AVAILABLE

Response profiles, multivariate analysis, and mineral water composition assays (PDF). This material is available free of charge via the Internet at <http://pubs.acs.org>.

Received for review June 9, 2008. Accepted July 28, 2008.

AC801165V